Investigating the Potential of Alkali Metal Plumba-*closo*-Dodecaborate ($B_{11}H_{11}Pb^{2-}$) Salts as Solid-State Battery Electrolytes

Thomas A. Hales, Kasper T. Møller †, Terry D. Humphries, Anita M. D'Angelo ‡, Craig E. Buckley, Mark Paskevicius *

Physics and Astronomy, Curtin University, GPO Box U1987, Perth, WA 6845, Australia

KEYWORDS

Ion Conductivity, Battery, Solid-State Electrolyte, Energy Storage, Heavy Metal, Borate

ABSTRACT

Metal dodecaborate salts have been identified as a new class of ion conductor that are highly tuneable. A [B−H] unit within the dodecaborate anion can be replaced with a Pb atom to create a dipole and anisotropy within the anion to tune the crystal structure of alkali metal salts, enhancing ion conductivity for solid-state electrolyte (SSE) applications in batteries. $Li_2B_{11}H_{11}Pb{\cdot}xH_2O$ shows superionic conductivity up to ~ 7 mS cm^{-1} at 120 °C, proving it comparable to state-of-the-art $LiCB_{11}H_{12}$ at these temperatures. Dehydration of the Li-salt occurs above 120 °C causing changes in the crystal structure and a decrease in the ion conductivity. $Na_2B_{11}H_{11}Pb{\cdot}xH_2O$ shows modest ion conductivity (0.01 mS cm^{-1} at 170 °C), whereas the potassium salt shows conductivities

below 1 x 10^{-5} mS cm^{-1}. The $B_{11}H_{11}Pb^{2-}$ analogues are proposed to be inferior ion conductors to the $CB_{11}H_{12}^{-}$ varieties due to the divalent $B_{11}H_{11}Pb^{2-}$ anion causing stronger bonding between the cation and anion, possibly higher energy required to move from position to position within the crystal structure. Despite this, the insertion of a lead atom into the dodecaborate cage shows promise in allowing high ion conductivity in the solid-state.

INTRODUCTION

Batteries are becoming more prevalent as large-scale energy storage devices due to the increased use of intermittent energy sources including wind and solar. Classical lithium ion batteries contain three main components; a lithium-doped metal oxide cathode (e.g. CoO_2), a graphite anode, and a liquid electrolyte such as $LiPF_6$ in an organic solvent (e.g. ethylene carbonate).[1] Due to the fluidic nature of liquid electrolytes they have high ion conductivity but the organic solvents are prone to leakage and are often volatile and flammable.[2] Furthermore, the temperature range in which these solvents are in a liquid state is limited (e.g. −20 – 60 °C) so there are freezing and evaporation risks.[3–5] To counteract these drawbacks, and assess alternate battery chemistries, investigations into solid-state electrolytes have recently been revived. Inorganic solids have been known to be good ion conductors since the 19th century, however, it is only recently that they have come to prevalence due to the search for alternatives to traditional liquid electrolytes in battery applications.[6] Studies have shown that solid electrolytes can be more effective due to the possibility for higher power densities. [7]

Boranes have been known for over 100 years since their discovery by Alfred Stock in 1912 and exist from the simplest BH_3 molecule to larger polyhedral borane cages,[8] such as the *closo*-dodecaborate $[B_{12}H_{12}]^{2-}$ dianion. A major characteristic of boranes is their electron deficient nature

and also 3-centre 2-electron bonding with bridging hydride for molecules with multiple boron atoms, where these factors help define much of the chemistry in which boranes partake.[9,10] This allows the formation of highly stable multi-vertex borane cages.

One borate of particular interest is the *closo*-dodecaborate dianion $[B_{12}H_{12}]^{2-}$ that has an icosahedral structure with a high degree of symmetry, where metal salts of this anion have shown to have high ion conductivity of the cation.[11,12] Substituting a boron atom with a carbon forms a 12-vertex monocarborate anion $[CB_{11}H_{12}]^{-}$, which reduces the charge of the anion to monovalent, due to the extra proton in the carbon atom. The asymmetry also creates a dipole within the anion due to the difference in electronegativity between the respective elements.[13,14] The ion conductivity of $[CB_{11}H_{12}]^{-}$ salts is higher than their borate analogues at lower temperatures,[12] partly hypothesised to be due to the reorientational motion of the asymmetric anion.[15] Despite the promising ion conductivity of $[CB_{11}H_{12}]^{-}$ salts, there has been little research into the ion conductivity by incorporating other group 14 heteroatoms into the 12-vertex borate cage.

Replacing a [B−H] unit in the $[B_{12}H_{12}]^{2-}$ structure with a Pb atom maintains the −2 charge on the anion and also produces a dipole within the molecule. Pb has a larger atomic radius (2.49 Å) compared to C (1.90 Å) and significantly changes the charge distribution in the anion.[16] Thus, it is postulated that the structural and electronic changes to the anion could affect the ion conductivity of alkali metal salts of plumba-*closo*-dodecaborates, which may allow them to be used as SSEs in battery applications. The synthesis of $B_{11}H_{11}Pb^{2-}$ was reported in 1992, where Chapman *et. al.* published a method where trimethylammonium *nido*-undecaborate ($(CH_3)_3NHB_{11}H_{14}$) was reacted with lead(II) chloride in basic conditions at room temperature.[17] Despite the toxicity of $PbCl_2$, this synthetic method does not require any additional or extreme conditions so it is a preferential route.[18]

This paper focuses on the synthesis and characterisation of alkali metal salts of the plumba-*closo*-dodecaborate dianion ($B_{11}H_{11}Pb^{2-}$) and their use as prospective solid-state electrolytes. The substitution of a carbon atom for a boron atom, the lightest group 14 element, has been proven to improve ion conductivity. As such, substituting with other group 14 elements may also demonstrate improved ion conductivity. Lead is already widely used in Pb-acid batteries and due to the full solid-state nature of the cell, the battery is easier to dispose of and spill risk is eradicated, as a result, the risk of lead poisoning is lower than current lead containing batteries.[19]

EXPERIMENTAL

Materials and Methods

Nuclear Magnetic Resonance (NMR) spectroscopy was performed on a Bruker AVANCE III 400 MHz spectrometer (128.4 MHz for ^{11}B) with proton decoupled spectra referenced to $BF_3{\cdot}OEt_2$. There is a pronounced background signal in ^{11}B spectra due to the presence of borosilicate probe coil inserts in the instrument. An ^{11}B background scan is shown in Figure S1. Fourier Transform Infrared Attenuated Total Reflectance (FTIR-ATR) spectroscopy using a diamond crystal was performed on all samples on a ThermoFisher Nicolet Summit FTIR Spectrometer. Due to the hygroscopic nature of the compounds, air exposure was minimised to ~ 2 seconds. Each sample was measured from 400 – 4000 cm^{-1} and averaged over 16 scans. Differential scanning calorimetry (DSC) and Thermogravimetric analysis (TGA) were performed using a Netzsch STA 449 F3 Jupiter apparatus. The samples (~4 mg) were placed in a sealed aluminium crucible and heated from 40 to 400 °C (10 °C min^{-1}) in an argon flow of 40 mL min^{-1}. The temperature and sensitivity of the DSC was calibrated using In, Zn, Sn, Bi, and CsCl reference materials, resulting in a temperature accuracy of ± 0.2 °C, while the balance has an accuracy of ± 20 µg. Residual Gas

Analysis – Mass Spectroscopy (RGA) was performed on all samples by adding ~ 10 mg to a sealed Swagelok reactor. The reactor was then placed under vacuum and heated at 5 °C min^{-1} from 25 °C to 350 °C. The residual gases evolved from the heating were measured using an RGAPro-2500 (Hy-Energy LLC).

Temperature Programmed Photographic Analysis (TPPA) was performed on the samples by pressing the compounds into pellets (Diameter - 6 mm, Thickness – 1 mm, Pressure – 9800 N (346.6 MPa)) in an inert argon atmosphere. The pellet was placed within a sealed test tube filled with argon gas. The test tube was placed within an aluminium block, which is heated by resistive heating at a rate of 10 °C min^{-1} until 350 °C. The pellet was recorded using a camera to elucidate any physical changes through the heating process.

Electrochemical Impedance Spectroscopy (EIS) was measured using a ZIVE SP1 instrument. The compounds were pressed into pellets, with a diameter of 6 mm and thickness of ~ 1 mm, by applying a pressure of 9800 N (346.6 MPa) in an inert argon atmosphere. A pellet was placed between 2 gold wafers (0.1 mm thickness) and loaded into Teflon sealed sample cells with stainless steel electrodes, which was sealed to maintain an inert atmosphere throughout the test. The data was collected using AC voltage from 1 MHz to 10 Hz. To elucidate the ion conductivity (σ) from the data, the x-intercept (R_{real}) of the Nyquist plot was determined using a known literature method, see Figure S2. [11]

Linear Sweep Voltammetry (LSV) was performed to determine the oxidative stability limit of the sample against Li metal. The method used was based on a method proposed by Han *et. al.* and Asakura *et. al.*.[20,21] $Li_2B_{11}H_{11}Pb{\cdot}xH_2O$ was mixed with graphite (Sigma Aldrich), previously heated to 550 °C under vacuum for 12 h, in a weight ratio of 75:25 by grinding 5 times with a mortar and pestle. 3 mg of the mixture was layered on top of 40 mg of pure sample and pressed

together at 19600 N (693.2 MPa) in an inert argon atmosphere to form a two layered pellet. This pellet was sandwiched to form an Al/Pt/Sample+C/Sample/Li configuration, which was sealed within an air tight Teflon cell. LSV was conducted twice at 60 °C with a scan rate of 50 μV s^{-1} from 1 V to 5.2 V. The oxidative stability of the material vs Li^+/Li was determined from the intersection point of two linear lines with $R^2 > 0.99$ (the background and the oxidative current).[21]

In situ and ex situ Synchrotron Radiation – X-Ray Diffraction (SR-XRD) data were collected on the powder diffraction (PD) beamline at the Australian Synchrotron using a Mythen strip detector with at a scan rate of 30 secs $scan^{-1}$ using a wavelength of 0.590958(5) Å, refined using NIST LaB_6 660b.[22] All samples were packed in borosilicate capillaries (outer diameter – 0.7mm) and sealed to ensure an argon atmosphere. The samples were heated to 600 K using a hot air blower at 5 °C min^{-1}. Sample temperatures were calibrated against the known lattice parameter of silver as a function of temperature.[23] Crystallographic indexing was performed in Topas v.5 (Bruker, Germany).

Density Functional Theory (DFT) was performed using the B3LYP hybrid functional with a LanL2MB basis set, in order to be able to compute the large number of electrons in the Pb atom.[24–26] The calculations were performed using the software Gaussian G09W optimising geometry and anion energy.[27] Electrostatic Potential (ESP) surfaces were mapped at an isovalue of 5.40 x 10^{29} electrons m^{-3}.

Materials

Lithium hydroxide (98%, −4+14 mesh, anhydrous, Alfa Aesar), anhydrous sodium hydroxide (reagent grade, ≥98%, pellets, Sigma-Aldrich), potassium hydroxide (technical, ≥85% powder, Sigma-Aldrich), lead (II) chloride (98%, Sigma-Aldrich), hydrochloric acid (37%, Fisher), nitric

acid (70%, Sigma-Aldrich), methyltriphenylphosponium bromide (98%, Sigma-Aldrich) were all used as purchased or diluted to desired concentrations using Milli-Q water. $(CH_3)_3NHB_{11}H_{14}$ was prepared using the method of Dunks *et. al.* from sodium borohydride (98% (0.5% $MgCO_3$) Sigma-Aldrich) and 1-bromopentane (98%, Sigma-Aldrich) in diglyme (99.5%, anhydrous, Sigma-Aldrich).[28] The synthesis involves dissolving sodium borohydride in diglyme and heating with added 1-bromopentane to 105 °C for 4h. All samples were prepared in air but were stored in a glove box under an inert argon atmosphere.

Synthetic Procedures

Synthesis of $M_2B_{11}H_{11}Pb$ (M = Li, Na, K)

The method was adapted from Chapman *et. al.*[17] $(CH_3)_3NHB_{11}H_{14}$ (1.231 g, 6.37 mmol) was dissolved in aqueous *M*OH (45 mL, 2M, *M* = Li, Na, K) before $PbCl_2$ (3.713 g, 13.35 mmol) was added and stirred at room temperature for 4 hours. The grey suspension was filtered and the filtrate neutralised to pH 7 using HCl (1M). The resulting grey precipitate was filtered, and the filtrate dried using a rotary evaporator leaving a yellow solid product. The solid was dissolved in CH_3CN (20 mL), to remove the insoluble *M*Cl by-product, filtered and the filtrate dried once more at 150 °C yielding a pale yellow, highly hygroscopic solid, which was stored under an inert atmosphere ($Na_2B_{11}H_{11}Pb$ (0.7752 g, 2.02 mmol, 32% yield) ($Li_2B_{11}H_{11}Pb$ – 34% yield, $K_2B_{11}H_{11}Pb$ – 30% yield). ^{11}B $\{^1H\}$ NMR (128 MHz, CD_3CN, ppm) −3.5 (s, 1B), −5.4 (t, $^1J_{11B–207Pb}$ = 263 Hz, 5B), −10.8 (s, 5B). ^1H $\{^{11}B\}$ NMR (400 MHz, CD_3CN, ppm) 6.7 (s, 1H), 3.0 (s, 5H), 0.9 (t, $^2J^1{}_{H–}{}^{207}{}_{Pb}$ = 120 Hz, 5B). FTIR (ATR, cm^{-1}) 2420 (vs), 1600 (w), 1050 (m), 730 (m), 700 (w), 520 (m).

Synthesis of $(MePh_3P)_2B_{11}H_{11}Pb$

$[(CH_3)_3NH]B_{11}H_{14}$ (0.271 g, 1.40 mmol) was dissolved in *M*OH (20 mL, 2M) before $PbCl_2$ (1.514 g, 5.45 mmol) was added and stirred at room temperature for 4 hours. The grey suspension was filtered and the filtrate neutralised to pH 7 using HCl (1M) and filtered *in vacuo* once more. $MePh_3PBr$ (1.010 g, 2.83 mmol) was dissolved in milliQ H_2O (10 mL) and added to the filtrate. A yellow solid precipitated and was filtered, washed with milliQ H_2O (2 x 5 mL), and the resulting solid dried at 90 °C under vacuum for 4 hours ($(MePh_3P)_2B_{11}H_{11}Pb$, 0.8664 g, 0.971 mmol, yield 69 %). ^{11}B $\{^1H\}$ NMR (128 MHz, CD_3CN, ppm) −3.5 (s, 1B), −5.4 (m, 5B), −10.8 (s, 5B).

RESULTS AND DISCUSSION

The syntheses of $B_{11}H_{11}Pb^{2-}$ salts follow that of the analogous compound, $CB_{11}H_{12}^-$. This can be performed from the trimethylammonium salt of the *nido*-undecaborate anion ($(CH_3)_3NHB_{11}H_{14}$). A $[CB_{11}H_{12}]^-$ synthesis pathway proposed by Franken *et. al.,* uses chloroform to form dichlorocarbene, which is inserted into the *nido* cage to form the *closo* 12-vertex product,[29] and was recently made cost effective.[30] This method requires the use of an inert gas atmosphere (*e.g.* argon) at all stages due to the highly reactive carbene intermediate, which must be synthesised *in situ*. However, the formation of the lead analogue is simpler. Heavier group 14 elements such as lead and tin can form stable EX_2 (*E* = Group 14 element, *X* = Halide) compounds so, in the case of $PbCl_2$, the reaction can be performed in air. Alkali metal $B_{11}H_{11}Pb^{2-}$ salts are soluble in water and organic solvents such as dimethylsulfoxide (DMSO), acetone and acetonitrile.

An insoluble $B_{11}H_{11}Pb^{2-}$ salt can be isolated as shown in reactions 1 and 2.[31]

$$[(CH_3)_3NH][B_{11}H_{14}]_{(s)} + 4\ NaOH_{(aq)} + PbCl_{2\ (s)} \xrightarrow[RT\ 4h]{} Na_2B_{11}H_{11}Pb_{(aq)} + 2\ NaCl_{(aq)} + (CH_3)_3N_{(g)} + 4\ H_2O_{(l)} \quad (1)$$

$$Na_2B_{11}H_{11}Pb_{(aq)} + 2\ (CH_3)_4NCl_{(aq)} \longrightarrow [(CH_3)_4N]_2B_{11}H_{11}Pb_{(s)} + 2\ NaCl_{(aq)} \quad (2)$$

Figure 1 shows the electrostatic potential surface of varying borate and heteroborate anions calculated using Gaussian G09W software. Substituting a [B−H] unit with a heteroatom in the 12-membered boron cage produces a pronounced electrostatic dipole. This dipole may be responsible for improving the ion conductivity in $[CB_{11}H_{12}]^-$ compounds with respect to the unsubstituted $[B_{12}H_{12}]^{2-}$ anion.[32] Adding a lead atom into the cage also creates a dipole, similar to the $[CB_{11}H_{12}]^-$, with the main difference between the two anions being the valency, i.e. $[B_{11}H_{11}Pb]^{2-}$ is a divalent anion, whereas the $[CB_{11}H_{12}]^-$ is monovalent. Another difference is the *X*−B1 (*X* = B12, C, or Pb (see Figure 1)), distance, which increases, respectively, due to the size of the lead atom (4.338 Å) with respect to carbon (3.273 Å) or boron (3.437 Å) as theoretically calculated. However, the calculated overall size, measured from Pb−H1 (where H1 is hydrogen atom bonded to B1), of the $[B_{11}H_{11}Pb]^{2-}$ anion (5.503 Å) is a similar size to both the unsubstituted $[B_{12}H_{12}]^{2-}$ (H12−H1 = 5.833 Å) and the $[CB_{11}H_{12}]^-$ (CH−H1 = 5.524 Å). This is due to the fact that the smaller carbon atom sits further down into the cage, causing a degree of asymmetry. The $B_{12}H_{12}^{2-}$ anion is slightly bigger than the $B_{11}H_{11}Pb^{2-}$ due to the lack of hydrogen atom bonded to the Pb atom, as a result, there is an extra H atom in the full length of the unsubstituted $B_{12}H_{12}^{2-}$ anion. It is expected that cationic coordination to the anion will be impacted by the electrostatic dipole, affecting the solid-state crystal structure of the resulting alkali metal salts (for atomic coordination of the $B_{11}H_{11}Pb^{2-}$ anion as calculated see Table S1). The cationic coordination also depends on the level of coordinated water on the cation, which would buffer the distance between the cation and anion and may impact the mobility of the cation in the crystal.

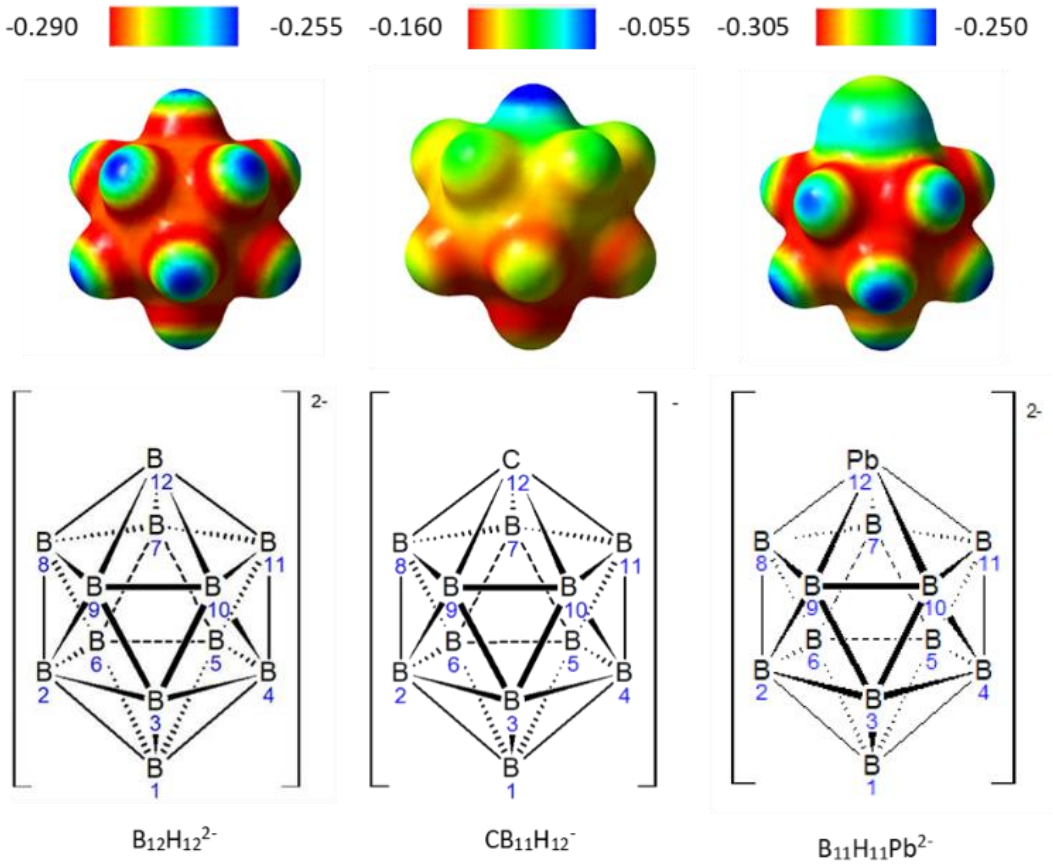

Figure 1. Electrostatic potential and structures without hydrogens of various anions using Density Functional Theory (DFT) and a B3LYP/LanM2MB basis set (Total Self-Consistent Field (SCF) Density (isovalue = 0.008)). NOTE: Pb atom in $B_{11}H_{11}Pb^{2-}$ is not protonated. The electrostatic potential is displayed in atomic units, where 1 au = 2.625 MJ/mol. A variation of this figure is provided in Figure S3 where the potentials are plotted against the same colour scale. Figure S4 also provides the Mulliken charges for $B_{11}H_{11}Pb^{2-}$.

FTIR spectroscopy data confirms that the spectra of the methyltriphenylphosphine ($MePh_3P^+$) $B_{11}H_{11}Pb^{2-}$ salt corresponds to previously published FTIR data (Figure S5).[17] This spectrum shows a large amount of signals in the low-wavenumber fingerprint region. These modes arise from the

additional bonding seen in the $MePh_3P^+$ cation that contains C-H, C=C aromatic and C-P bonds, in contrast to the alkali metal cations.[33] The corresponding IR active modes contribute to the large number of additional peaks in comparison to the alkali metal salts. The three alkali metal salts have very similar FTIR spectra with the characteristic B−H stretch at 2420 cm^{-1}. However, the lithium compound shows a stronger water signal at both 3500 and 1600 cm^{-1} compared to the sodium and potassium salts. These peaks correspond to an O−H stretch and H−O−H bend, respectively, which arise from coordinated water to the compounds in their crystal structure.[34] Furthermore, the FTIR spectra shows there is an absence of a Pb−H stretch meaning the Pb atom in the anion structure is not protonated as desired.[35] Furthermore, the Pb atom has a +2 oxidation state which is desirable and any protonation would lead to a higher, more unfavourable oxidation state, as determined by the inert pair effect.[36]

The ^{11}B NMR spectrum of the $B_{11}H_{11}Pb^{2-}$ anion shows three distinct signals at −3.5 (B1), −5.4 (B7−B11), and −10.8 ppm (B2−B6) (Figure 2). These resonances are shifted downfield from the non-substituted $B_{12}H_{12}^{2-}$ dianion which has a typical chemical shift of −15.4 ppm, with respect to a $BH_3{\cdot}OEt_2$ standard.[37,38] There are three chemical environments for boron within the anion and all hydrogen coupled signals are doublets ($^2J_{B-H}$ = 125.5 Hz) as each boron atom is bonded to a single hydrogen atom (see Figure S6c). ^{11}B integration shows a 1:5:5 ratio, revealing that the −3.5 ppm resonance corresponds to the antipodal boron (B1 – see Figure 1 for atom identification) atom with respect to the Pb heteroatom. The large downfield-shift of the antipodal boron (B1) is caused by the introduction of a heteroatom into the cage-like structure, which causes the largest amount of deshielding in the antipodal position.[39] The two upfield resonances correspond to the two different sets of five equivalent boron atoms (B2−B6 and B7−B11). The peak at −5.4 ppm is split further by coupling with a ^{207}Pb nuclei, which is also NMR active ($^1J_{B-Pb}$ = 265.1 Hz), confirming

that the peak at −5.4 ppm corresponds to boron atoms directly bonded to the lead atom (B7−B11). The splitting is noticeable because the ^{207}Pb nucleus has a relative natural abundance of 23% with the remainder of the stable isotopes being NMR inactive.[40] This gives an apparent triplet, as 23% of the $B_{11}H_{11}Pb^{2-}$ molecules show a doublet and 77% a singlet. These peaks have the same chemical shift, as a result, the spectrum shows a multiplet with three signals. There is a minor impurity peak at −16 ppm in the spectra, which correspond to the $B_{11}H_{11}^{2-}$ anion that is formed by premature closure of the *nido*-cage without the insertion of the Pb atom (Figure S6b). Other impurities found during synthetic process include unreacted $B_{11}H_{14}^{-}$ precursor (δ_{11B} = 13.7, −15.5 and −16.9) and its oxidation product, $B_{11}H_{12}O^{-}$, at 12.8, 11.3, 4.4, −7.0, 14.2, −16.4 and −29.1 ppm.[41,42] The concentrations of these impurities are low and not thought to greatly affect the properties of the bulk materials, as from ^{11}B NMR spectroscopy and SR-XRD, we believe the purity to be >95%. The purity achieved is similar to other materials previously screened for ionic conductivity.[43] All NMR spectra can be found in the supporting information (Figure S6).

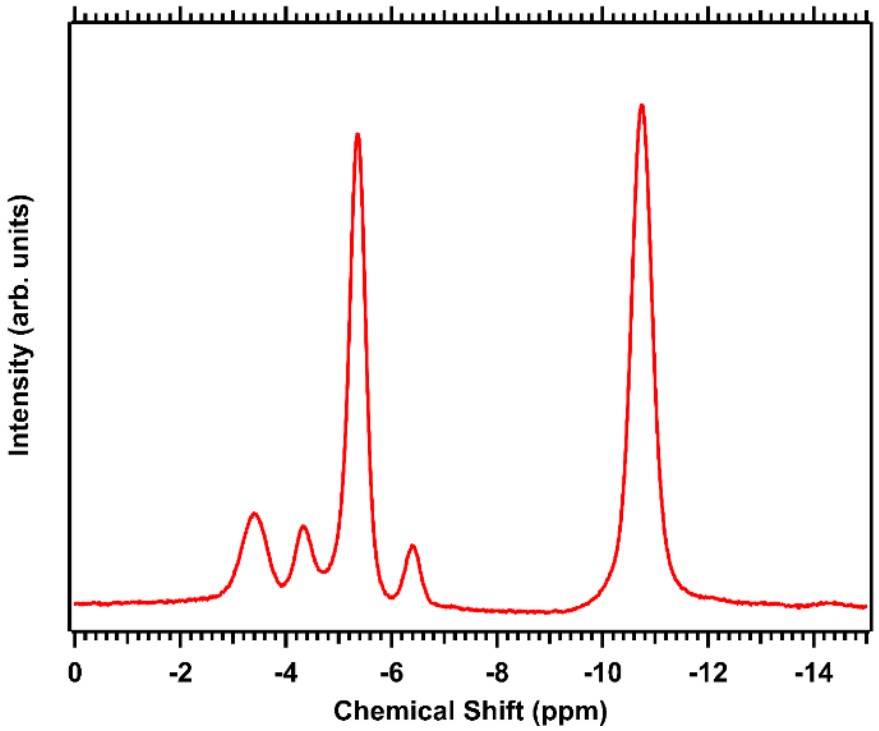

Figure 2. ^{11}B $\{^{1}H\}$ NMR spectrum of $Na_2B_{11}H_{11}Pb$ in CD_3CN - −3.5 (s, 1B, B1), −5.4 (m, $^{1}J_{11B-207Pb}$ = 263 Hz, 5B, B7−B11), −10.8 (s, 5B, B2−B6).

The *in-situ* SR-XRD of $Li_2B_{11}H_{11}Pb$, performed during thermal treatment, identifies a mixture of at least three different compounds at room temperature (Figure 3), considered to be a mixture of different hydrates of $Li_2B_{11}H_{11}Pb$. α-$Li_2B_{11}H_{11}Pb{\cdot}xH_2O$ (blue circles) disappears at ~120 °C on heating, causing an increase in scattered intensity in β-$Li_2B_{11}H_{11}Pb{\cdot}xH_2O$ (green diamond), indicating a potential dehydration event. A similar event occurs at ~170 °C when β-$Li_2B_{11}H_{11}Pb{\cdot}xH_2O$ disappears and an increase in scattered intensity is seen in γ-$Li_2B_{11}H_{11}Pb{\cdot}xH_2O$ (purple triangles).

The α-phase could not be indexed but β-$Li_2B_{11}H_{11}Pb{\cdot}xH_2O$ was indexed in space group $P4_2nm$ (102), however, determining the atomic positions was not possible due to the large discrepancy between the combined scattering power of the $B_{11}H_{11}Pb^{2-}$ anion with the electron-poor Li^{+} cation. γ-$Li_2B_{11}H_{11}Pb{\cdot}xH_2O$ persists until 300 °C where decomposition into Pb metal occurs slightly

below the reported melting point at 327.5 °C.[35] This is a lower temperature than unsubstituted $Li_2B_{12}H_{12}$, which shows that it is less stable.[44] The lead is partially molten in the X-ray beam as indicated by the weak crystalline peaks (red squares) coupled by the broad non-crystalline scattering halo at $2\theta = 12°$, indicative of a disordered molten phase. All samples see the freezing of lead metal during cooling at ~ 190 °C, which is corroborated by an exothermic event seen in the DSC analysis of the compounds (Figure S7). This is vastly lower than the melting point of lead metal. Possible reasons for this could be the atmosphere within the capillary preventing the crystallisation of the solid, or the amalgamation of the alkali metals into Pb metal after decomposition of the borate causes the reduction of the melting point, however, not to the level seen in this experiment.[45] A minor impurity of lithium chloride (LiCl) also persists throughout the heating ramp, resulting from the slight solubility of lithium chloride in acetonitrile during synthesis. Other solvents, such as acetone, with lower solubilities of lithium chloride, are not used as they cause the $B_{11}H_{11}Pb^{2-}$ anion to decompose.

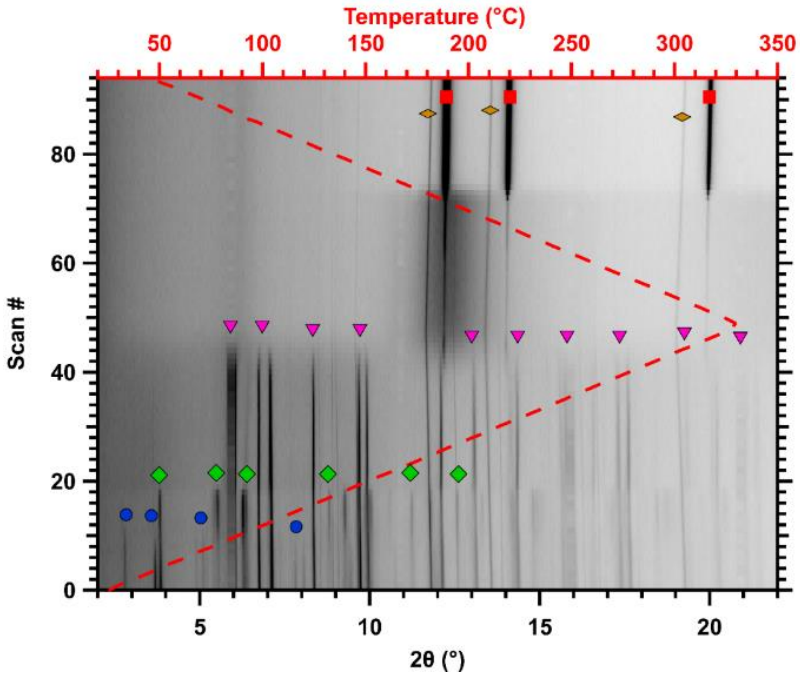

Figure 3. *In-situ* SR-XRD of dried $Li_2B_{11}H_{11}Pb$ under sealed Ar atmosphere and heated to 327 °C at 5 °C min^{-1} – Blue circle = α-$Li_2B_{11}H_{11}Pb{\cdot}xH_2O$, Green Diamond = β-$Li_2B_{11}H_{11}Pb{\cdot}xH_2O$, Pink Triangle = γ-$Li_2B_{11}H_{11}Pb{\cdot}xH_2O$, Red Square = Pb metal, Orange Diamond = LiCl.

The *in-situ* SR-XRD data for $Na_2B_{11}H_{11}Pb$ reveals a first decomposition of *α*-$Na_2B_{11}H_{11}Pb{\cdot}xH_2O$ into an amorphous phase, signified by a halo at 210 °C, before full decomposition into lead metal at ~ 300 °C. Sodium chloride is present as an impurity throughout the heating and cooling process (Figure 4a). Once more, the presence of molten lead occurs at a lower temperature than its standard melting point. The *α*-$Na_2B_{11}H_{11}Pb$ shows no dehydration in the initial heating which differs to the lithium salt. The initial phase *α*-$Na_2B_{11}H_{11}Pb{\cdot}xH_2O$ could not be indexed, possibly due to a mixture of different compounds or hydrates. The potassium analogue behaves similarly to the sodium variant (Figure 4b). The initial phase, *α*-$K_2B_{11}H_{11}Pb{\cdot}xH_2O$, decomposes at 220 °C into an amorphous compound which are notoriously

difficult to identify, whilst molten Pb forms at 310 °C.[38] As with the lithium salt, both the sodium and potassium salts freeze at 190 °C.

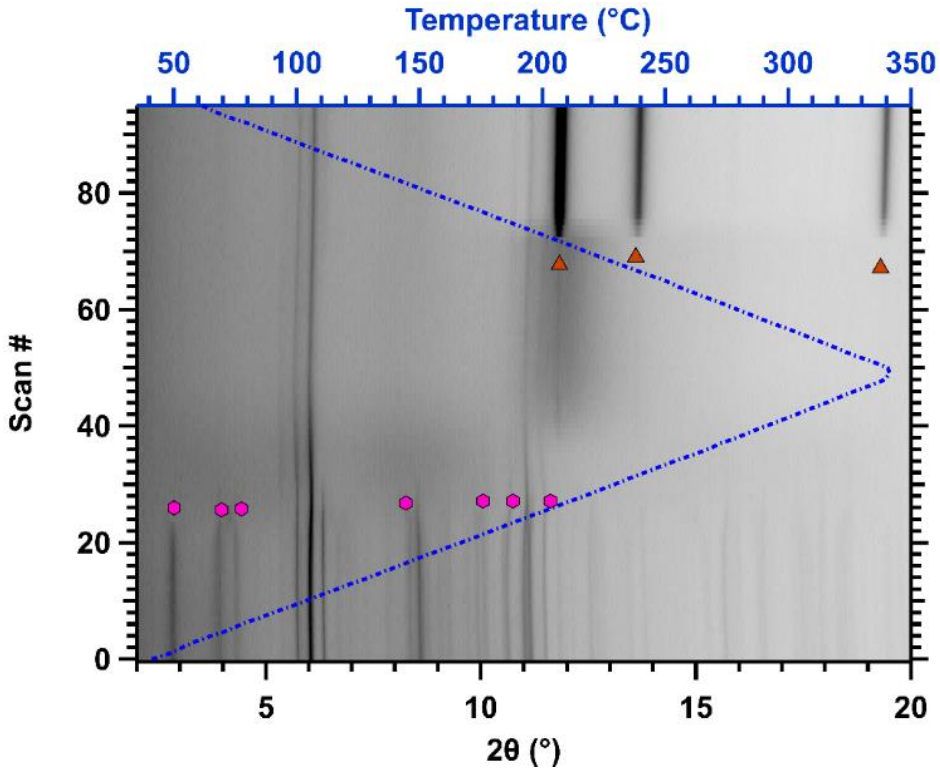

Figure 4a. *In-situ* SR-XRD of dried $Na_2B_{11}H_{11}Pb$ under sealed Ar atmosphere and heated to 327 °C at 5 °C min^{-1} – Pink circle = α-$Na_2B_{11}H_{11}Pb.xH_2O$, Brown Triangle = Pb metal.

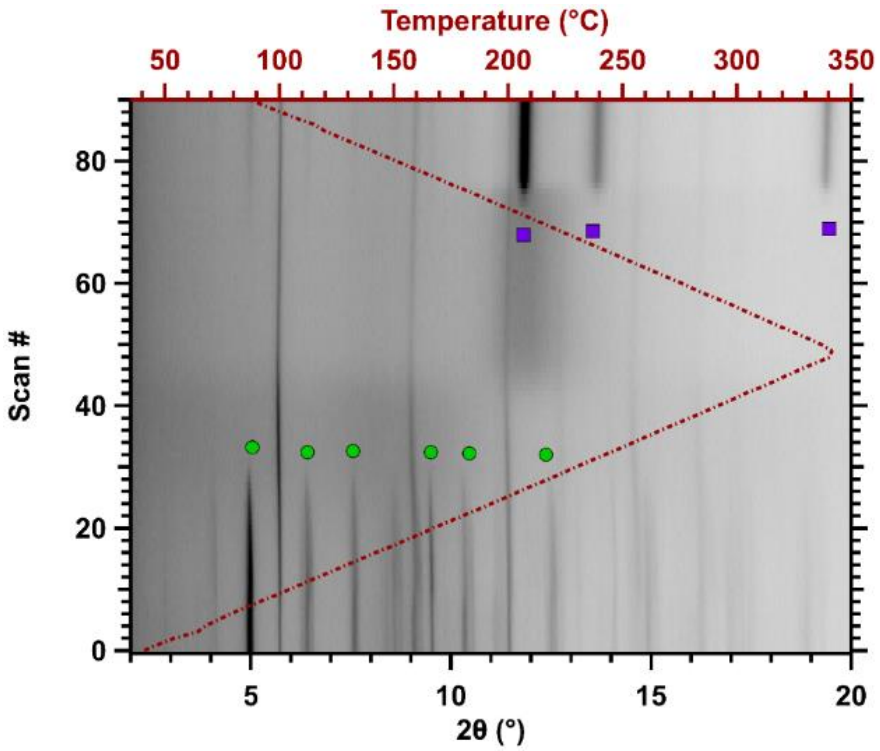

Figure 4b. *In-situ* SR-XRD of dried $K_2B_{11}H_{11}Pb$ under sealed Ar atmosphere and heated to 327 °C at 5 °C min^{-1} – Green Circle = α-$K_2B_{11}H_{11}Pb.xH_2O$, Blue Square = Pb metal.

Residual Gas Analysis (RGA) was performed on the different salts dried at both 90 °C and 150 °C with the water and hydrogen gas intensities being particularly probed (Figure 5). When the samples are dried at 90 °C *in vacuo*, a large amount of water was released for all samples above 90 °C. However, drying at 150 °C removed this coordinated water and reveals a release of water at higher temperatures, $Li_2B_{11}H_{11}Pb$ – 160 °C, $Na_2B_{11}H_{11}Pb$ and $K_2B_{11}H_{11}Pb$ – 240 °C. The evolution of hydrogen gas from a sample indicates the decomposition of the borate cage. The presence of the coordinated water (dried at 90 °C) causes decomposition at a lower temperatures for all salts as they begin the evolution of hydrogen gas at ~ 150 °C. Once the majority of this coordinated water has been removed (dried at 150 °C), the decomposition of the compounds occur

at a much higher temperature for all compounds, $Li_2B_{11}H_{11}Pb$ – 220 °C, $Na_2B_{11}H_{11}Pb$ – 260 °C and $K_2B_{11}H_{11}Pb$ – 270 °C.

Temperature Programmed Thermal Analysis of $Li_2B_{11}H_{11}Pb$ (Figure S8a) shows slight discolouration of the pale yellow pellet at ~ 120 °C which correlates with the dehydration observed in the *in-situ* XRD. Further discolouration proceeds at ~ 220 °C until the sample becomes black at ~300 °C, which signified full decomposition as seen in the *in-situ* XRD. $Na_2B_{11}H_{11}Pb$ shows decolouration at 210 °C which correlates with the *in-situ* XRD observations (Figure S8b). Further darkening of the pellet continues upon heating coinciding with the evolution of hydrogen as seen in the RGA until 310 °C which correlates to its decomposition shown by XRD. The potassium salt behaves in a similar manner to the sodium analogue with discolouration beginning at ~ 200 °C and full darkening of the pellet at 305 °C which coincides with the decomposition seen in the *in-situ* XRD.

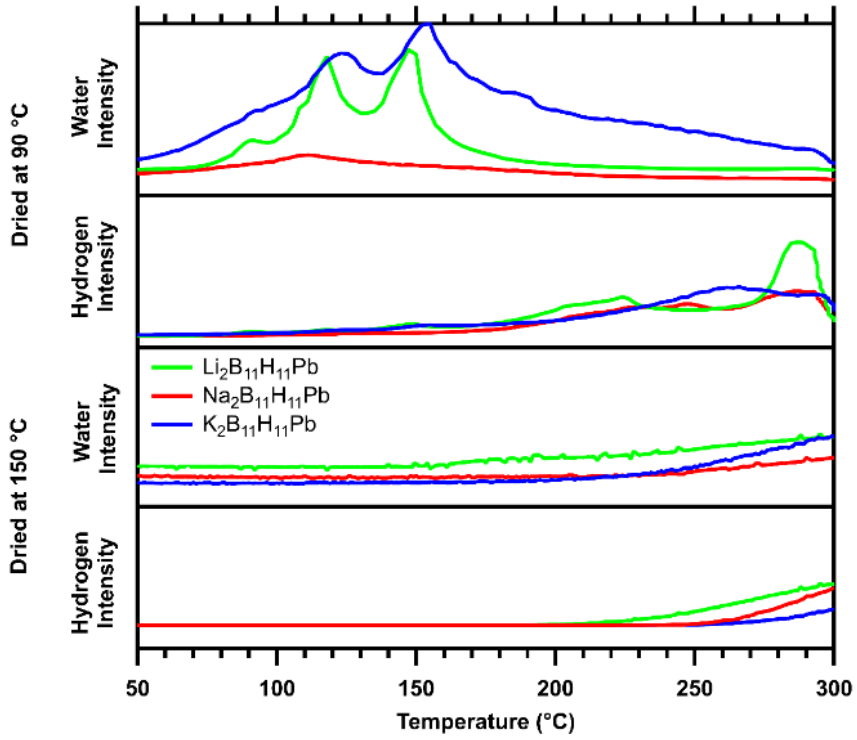

Figure 5. RGA Analysis of $Li_2B_{11}H_{11}Pb$, $Na_2B_{11}H_{11}Pb$ and $K_2B_{11}H_{11}Pb$ dried at 90 and 150 °C, heating at 5 °C min^{-1}.

Measuring the ion conductivity of a sample is the primary analytic technique to determine the potential of a compound as a solid-state electrolyte. $Li_2B_{11}H_{11}Pb{\cdot}xH_2O$ represents the best performing ion conductor in this study, reaching superionic conductivity (> 1 mS cm^{-1}) above 90 °C. Above 120 °C, the ion conductivity decreases again, which corresponds to the initial dehydration step of α-$Li_2B_{11}H_{11}Pb{\cdot}xH_2O$ observed in the *in-situ* SR-XRD. Between 90 - 120 °C $Li_2B_{11}H_{11}Pb$ has a greater ion conductivity than the pristine $B_{12}H_{12}^{2-}$ anion (see Figure 6a). However, the low conductivity at cooler temperatures (T < 70 °C), introduces limitations of $Li_2B_{11}H_{11}Pb{\cdot}xH_2O$ when compared to $LiCB_{11}H_{12}$. At 40 °C, $LiCB_{11}H_{12}$ has an ion conductivity of ~ 0.3 mS cm^{-1} whereas $Li_2B_{11}H_{11}Pb{\cdot}xH_2O$ is three orders of magnitude lower at 1 µS cm^{-1} as seen in Figure 6a. $Li_2B_{11}H_{11}Pb$ was heated to 100, 150, 200 and 310 °C to determine the stability of the

compound through heating. The ^{11}B {^{1}H} NMR spectra (Figure S6k) shows no anion degradation up to 200 °C which is higher than the temperatures at which the ion conductivity was measured. At 310 °C the anion has fully decomposed, matching the *in-situ* SR-XRD results.

One major difference between $CB_{11}H_{12}^-$ and $B_{11}H_{11}Pb^{2-}$ anions is the valency, as the lead containing compound is a divalent anion, the electrostatic attraction between the lithium cations and the anions is increased as seen in Figure 1. Furthermore, the $[CB_{11}H_{12}]^-$ is able to be fully dehydrated, whereas the $B_{11}H_{11}Pb^{2-}$ anion is not as seen by FTIR spectroscopy and RGA of the sample.[13] Complete dehydration of alkali metal plumba-*closo*-dodecaborates before decomposition is difficult or not possible once hydrated. The strong charge density of Li^+ and Na^+ cations result in strong coordination of crystal water until high temperatures where the compounds are shown to decompose. This is well-known in this class of compounds with weakly coordinating anions.[12] Despite this, it has been shown that hydration of other metal borates such as $LiB_{11}H_{14}$ and $NaB_{11}H_{14}$ is beneficial towards their ion conductivity due to the creation of a low energy migration pathway through the anionic lattice.[46,47] One reason that the $LiCB_{11}H_{12}$ has exceptional ion conductivity is due to the high temperature polymorphic transition at ~160 °C to a super ion conducting phase with highly mobile anions and cations.[13] The $Li_2B_{11}H_{11}Pb{\cdot}xH_2O$ does not undergo a high temperature polymorphic transition and so, does not exhibit a step function change in ion conductivity as a function of temperature. The sodium analogue has comparatively poor ion conductivity reaching a maximum of ~ 10^{-5} S cm^{-1} at 170 °C. This is considerably lower than the respective $NaCB_{11}H_{12}$ and also the pristine $NaB_{12}H_{12}$ salt (Figure 6b). The potassium salt has very low ion conductivity around the detectable limit (max. 7 x 10^{-9} S cm^{-1} at 160 °C). This is vastly reduced compared to its contemporaries, KB_3H_8 (3.4 × 10^{-7} S cm^{-1} at 150 °C), $KB_{11}H_{14}$ (1.2 x 10^{-4} S cm^{-1} at 150 °C) and $KCB_{11}H_{12}$ (3.2 x 10^{-4} S cm^{-1}) .[46,48,49]

Linear sweep voltammetry (LSV) was performed on $Li_2B_{11}H_{11}Pb$ to assess the oxidative stability of the compound. This shows the electrochemical limit at which the compound is irreversibly oxidised and therefore the working range of the materials. The limit was found to be 2.3 V vs Li^+/Li which is comparable to other borate salts such as $LiBH_4$, which has a slightly lower oxidative stability of 2.2 V vs Li^+/Li and $LiB_{11}H_{14}.xH_2O$ which is higher at 2.9 V vs Li^+/Li (Figure S9).[21,46] The LSV scan shows a negative initial current and a large positive current after the oxidative stability limit is seen. This is due to the addition of carbon in the cell, which increases background capacitive current, but also increases the accuracy of the oxidative stability limit.[21] Further investigations could involve the investigation of full cells. Possible cathode materials could include Ti_2S for Li and Na batteries.[50,51]

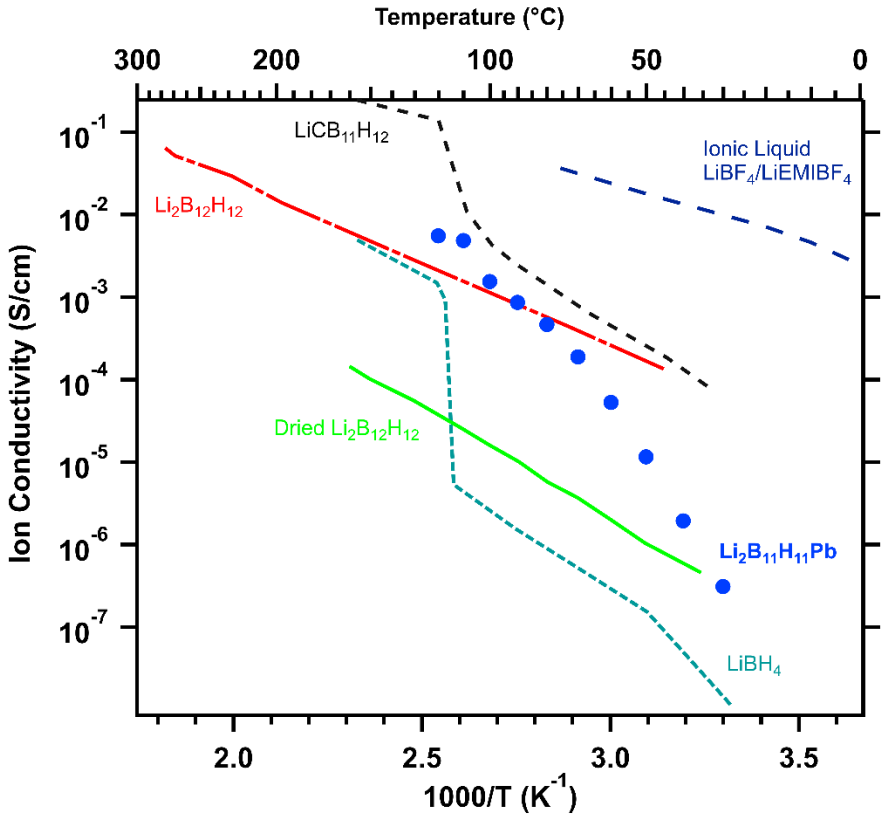

Figure 6a. Ion conductivity of various solid state Li^+ borate salts. [13,52–55,56]

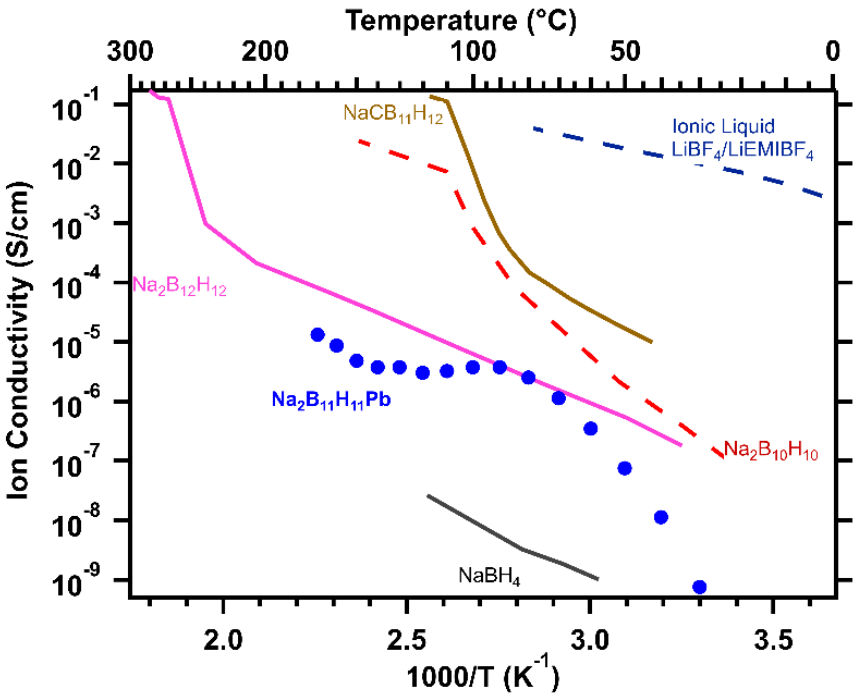

Figure 6b. Ion conductivity of various solid state Na^+ borate salts. [13,52–55]

CONCLUSIONS

A variety of group 1 metal plumba-*closo*-dodecaborate salts were successfully synthesised from trimethylammonium *nido*-undecaborate confirmed using ^{11}B NMR and FTIR spectroscopies. Further, investigation into the properties of this family of compounds using SR-XRD has shown that the crystal structures of these salts are internally different with the space group of $Li_2B_{11}H_{11}Pb$ being identified as $P4_2nm$ (102). The full crystal structure could not be identified due to the large disparity in the scattering power of the large $B_{11}H_{11}Pb^{2-}$ anions and small Li^+ cations. The primary focus of this paper was the identification of these compounds as potential ion conductors to be used in full solid-state battery cells. It has been found that $Li_2B_{11}H_{11}Pb{\cdot}xH_2O$ has good ion conductivity of > 1 mS cm^{-1} at temperatures of 90 – 120 °C to a maximum of 7 mS cm^{-1} at 120 °C. At higher temperatures, the ion conductivity decreases and this coincides with dehydration of

the salt as seen by *in-situ* SR-XRD and confirmed by the release of water vapour seen in the RGA-MS of the sample. Even though, it is surmised that is the divalent nature of the anion is the reason why the ion conductivity is lower than the $[CB_{11}H_{12}]^-$ variant, there are other factors such as the hydration level and other structural factors which could cause a weaker performance. However, due to the reactive and unstable nature of the anion, further adaptation to the anion was not possible to reduce the valency. Other cations such as Na^+ and K^+ were also synthesised, however, these show poor ion conductivity in comparison to the Li^+ variant and other solid-state borate compounds.

In conclusion, we do not believe that plumba-dodecaborate salts ($B_{11}H_{11}Pb^{2-}$) would be suitable as solid-state electrolytes without further development due to their ionic conductivity at room temperature and thermal stability in comparison to their contemporaries, such as $CB_{11}H_{12}^-$ salts. However, further development into these materials, for example through ball milling, could improve their performance and as a result their viability. A study into the dynamics of the conduction pathway using QENS or *in* situ NMR would also help gather additional information around this novel class of materials. Future work could include inserting different metals in the borate cage to reduce the charge of the anion to -1 similar to the 12-vertex carborane.

ASSOCIATED CONTENT

Supporting Information contains NMR spectroscopy, Nyquist plot, calculated anion atomic coordinates, FTIR spectroscopy, DSC, TPPA and LSV data.

AUTHOR INFORMATION

Corresponding Author

* Mark Paskevicius – m.paskevicius@curtin.edu.au

Present Addresses

† Kasper Møller – Physics and Astronomy, Curtin University, GPO Box U1987, Perth, WA 6845, Australia and Department of Biological and Chemical Engineering, Aarhus University, Aabogade 40, Aarhus DK-8200, Denmark

‡ Anita D'Angelo – Australian Synchrotron (ANSTO), Clayton, VIC 3168, Australia.

Author Contributions

The manuscript was written through contributions of all authors. All authors have given approval to the final version of the manuscript.

Notes

Any additional relevant notes should be placed here.

ACKNOWLEDGMENT

TH acknowledges the support from Curtin International Postgraduate Research Scholarship (CIPRS) and Research Stipend Scholarship. KTM acknowledges the financial support from the Independent Research Fund Denmark (International Post doc Grant 8028-00009B) and the Carlsberg Foundation (Reintegration Fellowship CF19-0465). MP thanks the Australian Research Council (ARC) for a Future Fellowship (FT160100303). This research was undertaken on the Powder Diffraction beamline at the Australian Synchrotron, part of ANSTO.

REFERENCES

(1) Nishi, Y. Lithium Ion Secondary Batteries; Past 10 Years and the Future. *J. Power Sources*

2001, *100* (1–2), 101–106. https://doi.org/10.1016/S0378-7753(01)00887-4.

(2) Balakrishnan, P. G.; Ramesh, R.; Prem Kumar, T. Safety Mechanisms in Lithium-Ion Batteries. *J. Power Sources* **2006**, *155* (2), 401–414. https://doi.org/10.1016/j.jpowsour.2005.12.002.

(3) Wang, H.; Wang, G.; Yuan, S.; Ma, D.; Li, Y.; Zhang, Y. Fe3O4-Nanoparticle-Decorated TiO2 Nanofiber Hierarchical Heterostructures with Improved Lithium-Ion Battery Performance over Wide Temperature Range. *Nano Res.* **2015**, *8* (5), 1659–1668. https://doi.org/10.1007/s12274-014-0655-0.

(4) Plichta, E. J.; Behl, W. K. Low-Temperature Electrolyte for Lithium and Lithium-Ion Batteries. *J. Power Sources* **2000**, *88* (2), 192–196. https://doi.org/10.1016/S0378-7753(00)00367-0.

(5) Ma, S.; Jiang, M.; Tao, P.; Song, C.; Wu, J.; Wang, J.; Deng, T.; Shang, W. Temperature Effect and Thermal Impact in Lithium-Ion Batteries: A Review. *Prog. Nat. Sci. Mater. Int.* **2018**, *28* (6), 653–666. https://doi.org/10.1016/j.pnsc.2018.11.002.

(6) Funke, K. Solid State Ionics: From Michael Faraday to Green Energy - The European Dimension. *Sci. Technol. Adv. Mater.* **2013**, *14* (4), 043502. https://doi.org/10.1088/1468-6996/14/4/043502.

(7) Zhuiykov, S.; Ono, T.; Yamazoe, N.; Miura, N. High-Temperature NOx Sensors Using Zirconia Solid Electrolyte and Zinc-Family Oxide Sensing Electrode. *Solid State Ionics* **2002**, *152–153* (2), 801–807. https://doi.org/10.1016/S0167-2738(02)00331-4.

(8) Sivaev, I. B.; Bregadze, V. I.; Sjöberg, S. Chemistry of Closo-Dodecaborate Anion

[B12H12]2-: A Review. *Collect. Czechoslov. Chem. Commun.* **2002**, *67* (6), 679–727. https://doi.org/10.1135/cccc20020679.

(9) Green, J. C.; Green, M. L. H.; Parkin, G. The Occurrence and Representation of Three-Centre Two-Electron Bonds in Covalent Inorganic Compounds. *Chem. Commun.* **2012**, *48* (94), 11481–11503. https://doi.org/10.1039/c2cc35304k.

(10) Parry, R. W.; Edwards, L. J. Systematics in the Chemistry of the Boron Hydrides. *J. Am. Chem. Soc.* **1959**, *81* (14), 3554–3560. https://doi.org/10.1021/ja01523a018.

(11) Hansen, B. R. S.; Paskevicius, M.; Jørgensen, M.; Jensen, T. R. Halogenated Sodium-Closo-Dodecaboranes as Solid-State Ion Conductors. *Chem. Mater.* **2017**, *29* (8), 3423–3430. https://doi.org/10.1021/acs.chemmater.6b04797.

(12) Hansen, B. R. S.; Paskevicius, M.; Li, H. W.; Akiba, E.; Jensen, T. R. Metal Boranes: Progress and Applications. *Coord. Chem. Rev.* **2016**, *323*, 60–70. https://doi.org/10.1016/j.ccr.2015.12.003.

(13) Tang, W. S.; Unemoto, A.; Zhou, W.; Stavila, V.; Matsuo, M.; Wu, H.; Orimo, S. I.; Udovic, T. J. Unparalleled Lithium and Sodium Superionic Conduction in Solid Electrolytes with Large Monovalent Cage-like Anions. *Energy Environ. Sci.* **2015**, *8* (12), 3637–3645. https://doi.org/10.1039/c5ee02941d.

(14) Jørgensen, M.; Shea, P. T.; Tomich, A. W.; Varley, J. B.; Bercx, M.; Lovera, S.; Černý, R.; Zhou, W.; Udovic, T. J.; Lavallo, V.; *et al.* Understanding Superionic Conductivity in Lithium and Sodium Salts of Weakly Coordinating Closo-Hexahalocarbaborate Anions. *Chem. Mater.* **2020**, *32* (4), 1475–1487. https://doi.org/10.1021/acs.chemmater.9b04383.

(15) Udovic, T. J.; Matsuo, M.; Unemoto, A.; Verdal, N.; Stavila, V.; Skripov, A. V.; Rush, J. J.; Takamura, H.; Orimo, S. I. Sodium Superionic Conduction in Na2B12H12. *Chem. Commun.* **2014**, *50* (28), 3750–3752. https://doi.org/10.1039/c3cc49805k.

(16) Rahm, M.; Hoffmann, R.; Ashcroft, N. W. Atomic and Ionic Radii of Elements 1–96. *Chem. - A Eur. J.* **2016**, *22* (41), 14625–14632. https://doi.org/10.1002/chem.201602949.

(17) Chapman, R. W.; Kester, J. G.; Folting, K.; Streib, W. E.; Todd, L. J. Synthesis and Chemistry of B11H11Sn2- and Its Germanium and Lead Analogs. Crystal Structure of [B11H11SnCH3]PPh3CH3·CH2Cl2. *Inorg. Chem.* **1992**, *31* (6), 979–983. https://doi.org/10.1021/ic00032a011.

(18) Goyer, R. A. Lead Toxicity: Current Concerns. *Environ. Health Perspect.* **1993**, *100*, 177–187. https://doi.org/10.1289/ehp.93100177.

(19) Ruetschi, P. Review on the Lead-Acid Battery Science and Technology. *J. Power Sources* **1977**, *2* (C), 3–120. https://doi.org/10.1016/0378-7753(77)85003-9.

(20) Han, F.; Zhu, Y.; He, X.; Mo, Y.; Wang, C. Electrochemical Stability of Li10GeP2S12 and Li7La3Zr2O12 Solid Electrolytes. *Adv. Energy Mater.* **2016**, *6* (8), 1–9. https://doi.org/10.1002/aenm.201501590.

(21) Asakura, R.; Duchêne, L.; Kühnel, R. S.; Remhof, A.; Hagemann, H.; Battaglia, C. Electrochemical Oxidative Stability of Hydroborate-Based Solid-State Electrolytes. *ACS Appl. Energy Mater.* **2019**, *2* (9), 6924–6930. https://doi.org/10.1021/acsaem.9b01487.

(22) Black, D. R.; Windover, D.; Henins, A.; Filliben, J.; Cline, J. P. Certification of Standard Reference Material 660B. *Powder Diffr.* **2011**, *26* (2), 155–158.

https://doi.org/10.1154/1.3591064.

(23) Suh, I. K.; Ohta, H.; Waseda, Y. High-Temperature Thermal Expansion of Six Metallic Elements Measured by Dilatation Method and X-Ray Diffraction. *J. Mater. Sci.* **1988**, *23* (2), 757–760. https://doi.org/10.1007/BF01174717.

(24) Wadt, W. R.; Hay, P. J. Ab Initio Effective Core Potentials for Molecular Calculations. Potentials for Main Group Elements Na to Bi. *J. Chem. Phys.* **1985**, *82* (1), 284–298. https://doi.org/10.1063/1.448800.

(25) Hay, P. J.; Wadt, W. R. Ab Initio Effective Core Potentials for Molecular Calculations. Potentials for the Transition Metal Atoms Sc to Hg. *J. Chem. Phys.* **1985**, *82* (1), 270–283. https://doi.org/10.1063/1.448799.

(26) Hay, P. J.; Wadt, W. R. Ab Initio Effective Core Potentials for Molecular Calculations. Potentials for K to Au Including the Outermost Core Orbitale. *J. Chem. Phys.* **1985**, *82* (1), 299–310. https://doi.org/10.1063/1.448975.

(27) Frisch, M. J.; Trucks, G. W.; Schlegel, H. B.; Scuseria, G. E.; Robb, M. A.; Cheeseman, J. R.; Scalmani, G.; Barone, V.; Mennucci, B.; Petersson, G. A.; et al. Gaussian 09W, v. 7.0; Gaussian, Inc.: Wallingford, CT, 2009.

(28) Dunks, G. B.; Barker, K.; Hedaya, E.; Hefner, C.; Palmer-Ordonez, K.; Remec, P. Simplified Synthesis of B10H14 from NaBH4 via B11H14- Ion. *Inorg. Chem.* **1981**, *20* (6), 1692–1697. https://doi.org/10.1021/ic50220a015.

(29) Franken, A.; King, B. T.; Rudolph, J.; Roa, P.; Noll, B. C.; Michl, J. Preparation of [Closo-

CB11H12]-by Dichlorocarbene Insertion into [Nido-B11H14]-. *Collect. Czechoslov. Chem. Commun.* **2001**, *66* (8), 1238–1249. https://doi.org/10.1135/cccc20011238.

(30) Berger, A.; Buckley, C. E.; Paskevicius, M. Synthesis of Closo -CB 11 H 12 – Salts Using Common Laboratory Reagents. *Inorg. Chem.* **2021**, *60*, 14744–14751. https://doi.org/10.1021/acs.inorgchem.1c01896.

(31) Plešek, J.; Baše, K.; Mareš, F.; Hanousek, F.; Štíbr, B.; Heřmánek, S. Potential Uses of Metallocarborane Sandwich Anions for Analysis, Characterization and Isolation of Various Cations and Organic Bases. *Collect. Czechoslov. Chem. Commun.* **1984**, *49* (12), 2776–2789. https://doi.org/10.1135/cccc19842776.

(32) Fisher, S. P.; Tomich, A. W.; Lovera, S. O.; Kleinsasser, J. F.; Guo, J.; Asay, M. J.; Nelson, H. M.; Lavallo, V. Nonclassical Applications of Closo-Carborane Anions: From Main Group Chemistry and Catalysis to Energy Storage. *Chem. Rev.* **2019**, *119* (14), 8262–8290. https://doi.org/10.1021/acs.chemrev.8b00551.

(33) Daasch, L. W.; Smith, D. C. Infrared Spectra of Phosphorus Compounds. *Anal. Chem.* **1951**, *23* (6), 853–868. https://doi.org/10.1021/ac60054a008.

(34) Coates, J. Encyclopedia of Analytical Chemistry -Interpretation of Infrared Spectra, A Practical Approach. *Encycl. Anal. Chem.* **2004**, 1–23.

(35) Lide, D. R. *CRC Handbook of Chemistry and Physics*, 85th ed.; Ride, D., Ed.; CRC: Boca Raton, 2004.

(36) Seth, M.; Faegri, K.; Schwerdtfeger, P. The Stability of the Oxidation State +4 in Group 14 Compounds from Carbon to Element 114. *Angew. Chemie - Int. Ed.* **1998**, *37* (18), 2493–

2496.

(37) Garroni, S.; Milanese, C.; Pottmaier, D.; Mulas, G.; Nolis, P.; Girella, A.; Caputo, R.; Olid, D.; Teixdor, F.; Baricco, M.; *et al.* Experimental Evidence of Na2[B12H12] and Na Formation in the Desorption Pathway of the 2NaBH4 + MgH 2 System. *J. Phys. Chem. C* **2011**, *115* (33), 16664–16671. https://doi.org/10.1021/jp202341j.

(38) Paskevicius, M.; Jepsen, L. H.; Schouwink, P.; Černý, R.; Ravnsbæk, D. B.; Filinchuk, Y.; Dornheim, M.; Besenbacher, F.; Jensen, T. R. Metal Borohydrides and Derivatives-Synthesis, Structure and Properties. *Chem. Soc. Rev.* **2017**, *46* (5), 1565–1634. https://doi.org/10.1039/c6cs00705h.

(39) Teixidor, F.; Viñas, C.; Rudolph, R. W. Rules for Predicting the 11B NMR Spectra of Closo-Boranes and Closo-Heteroboranes. *Inorg. Chem.* **1986**, *25* (19), 3339–3345. https://doi.org/10.1021/ic00239a005.

(40) Komárek, M.; Ettler, V.; Chrastný, V.; Mihaljevič, M. Lead Isotopes in Environmental Sciences: A Review. *Environ. Int.* **2008**, *34* (4), 562–577. https://doi.org/10.1016/j.envint.2007.10.005.

(41) Tolpin, E. I.; Lipscomb, W. N. Fluxional Behaviour of B11H112-. *J. Am. Chem. Soc.* **1973**, *95* (7), 2384–2386. https://doi.org/10.1021/ja00788a058.

(42) Yang, X.; Jiao, H.; Rague Schleyer, P. Von. Structures of the 12-Vertex Oxa- and Thia-Nido -Dodecaborates and B 13 H 132 - : A Theoretical DFT / GIAO / NMR Investigation. *Inorg. Chem.* **1997**, *36* (21), 4897–4899.

(43) Payandeh, S. H.; Rentsch, D.; Łodziana, Z.; Asakura, R.; Bigler, L.; Černý, R.; Battaglia,

C.; Remhof, A. Nido-Hydroborate-Based Electrolytes for All-Solid-State Lithium Batteries. *Adv. Funct. Mater.* **2021,** *31* (18), 2010046. https://doi.org/10.1002/adfm.202010046.

(44) Pitt, M. P.; Paskevicius, M.; Brown, D. H.; Sheppard, D. A.; Buckley, C. E. Thermal Stability of Li2B12H12 and Its Role in the Decomposition of LiBH4. *J. Am. Chem. Soc.* **2013**, *135* (18), 6930–6941. https://doi.org/10.1021/ja400131b.

(45) Martelli, D.; Venturini, A.; Utili, M. Literature Review of Lead-Lithium Thermophysical Properties. *Fusion Eng. Des.* **2019**, *138* (September 2018), 183–195. https://doi.org/10.1016/j.fusengdes.2018.11.028.

(46) H. P. Souza, D.; Møller, K. T.; Moggach, S. A.; Humphries, T. D.; D'Angelo, A. M.; Buckley, C. E.; Paskevicius, M. Hydrated Alkali-B11H14salts as Potential Solid-State Electrolytes. *J. Mater. Chem. A* **2021**, *9* (26), 15027–15037. https://doi.org/10.1039/d1ta01551f.

(47) Jensen, T. R. The Mechanism of Mg2+ Conduction in Ammine Magnesium Borohydride Promoted by a Neutral Molecule. *Phys. Chem. Chem. Phys.* **2020**, *22* (17). https://doi.org/10.1039/d0cp00158a.

(48) Grinderslev, J. B.; Møller, K. T.; Yan, Y.; Chen, X. M.; Li, Y.; Li, H. W.; Zhou, W.; Skibsted, J.; Chen, X.; Jensen, T. R. Potassium Octahydridotriborate: Diverse Polymorphism in a Potential Hydrogen Storage Material and Potassium Ion Conductor. *Dalt. Trans.* **2019**, *48* (24), 8872–8881. https://doi.org/10.1039/c9dt00742c.

(49) Dimitrievska, M.; Wu, H.; Stavila, V.; Babanova, O. A.; Skoryunov, R. V.; Soloninin, A. V.; Zhou, W.; Trump, B. A.; Andersson, M. S.; Skripov, A. V.; Udovic, T. J. Structural and

Dynamical Properties of Potassium Dodecahydro-Monocarba-Closo-Dodecaborate: KCB11H12. *J. Phys. Chem. C* **2020**, *124* (33), 17992–18002. https://doi.org/10.1021/acs.jpcc.0c05038.

(50) Latroche, M.; Blanchard, D.; El, A.; Hauback, B. C.; Jensen, T. R.; Jongh, P. E. De; Kim, S.; Nazer, N. S.; Ngene, P.; Orimo, S.; *et al.* Full-Cell Hydride-Based Solid-State Li Batteries for Energy Storage. *International Journal of Hydrogen Energy* **2019**, *44*, 7875-7887. https://doi.org/10.1016/j.ijhydene.2018.12.200.

(51) Yoshida, K.; Sato, T.; Unemoto, A.; Matsuo, M.; Ikeshoji, T.; Udovic, T. J.; Orimo, S. Fast Sodium Ionic Conduction in Na 2 B 10 H 10 - Na 2 B 12 H 12 Pseudo-Binary Complex Hydride and Application to a Bulk-Type All-Solid-State Battery. *Applied Physics Letters* **2017**, 110, *103901*. https://doi.org/10.1063/1.4977885.

(52) He, L.; Li, H. W.; Nakajima, H.; Tumanov, N.; Filinchuk, Y.; Hwang, S. J.; Sharma, M.; Hagemann, H.; Akiba, E. Synthesis of a Bimetallic Dodecaborate LiNaB12H12 with Outstanding Superionic Conductivity. *Chem. Mater.* **2015**, *27* (16), 5483–5486. https://doi.org/10.1021/acs.chemmater.5b01568.

(53) Sadikin, Y.; Brighi, M.; Schouwink, P.; Černý, R. Superionic Conduction of Sodium and Lithium in Anion-Mixed Hydroborates Na3BH4B12H12 and (Li0.7Na0.3)3BH4B12H12. *Adv. Energy Mater.* **2015**, *5*, 1501016. https://doi.org/10.1002/aenm.201501016.

(54) Udovic, T. J.; Matsuo, M.; Tang, W. S.; Wu, H.; Stavila, V.; Soloninin, A. V.; Skoryunov, R. V.; Babanova, O. A.; Skripov, A. V.; Rush, J. J.; *et al.* Exceptional Superionic Conductivity in Disordered Sodium Decahydro-Closo-Decaborate. *Adv. Mater.* **2014**, *26* (45), 7622–7626. https://doi.org/10.1002/adma.201403157.

(55) Rickert, H. Solid Ionic Conductors: Principles and Applications. *Angew. Chemie Int. Ed. English* **1978**, *17* (1), 37–46. https://doi.org/10.1002/anie.197800371.

(56) Unemoto, A.; Yoshida, K.; Ikeshoji, T.; Orimo, S. Bulk-Type All-Solid-State Lithium Batteries Using Complex Hydrides Containing. *Materials Transactions* **2016**, *57* (9), 1639–1644. https://doi.org/10.2320/matertrans.MAW201601.